Pyrene Adsorption on a Ag(111) Surface

Eric Salomon, Marco Minissale, Francisco Romero Lairado, Stephane Coussan, Pierre Rousselot-Pailley, Francois Dulieu, Thierry Angot

THE JOURNAL OF PHYSICAL CHEMISTRY C
A JOURNAL OF THE AMERICAN CHEMICAL SOCIETY

pubs.acs.org/JPCC

Article

Pyrene Adsorption on a Ag(111) Surface

Eric Salomon,* Marco Minissale, Francisco Romero Lairado, Stephane Coussan, Pierre Rousselot-Pailley, François Dulieu, and Thierry Angot

Cite This: *J. Phys. Chem. C* 2021, 125, 11166−11174

Read Online

ACCESS | Metrics & More | Article Recommendations | Supporting Information

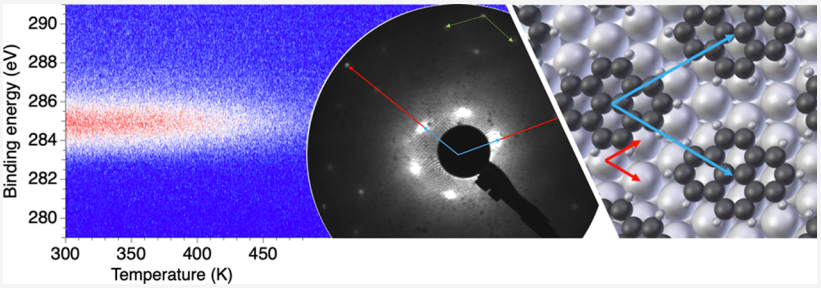

ABSTRACT: This work describes the adsorption of pyrene molecules on a Ag(111) surface. We first demonstrate that despite its high vapor pressure, pyrene molecules can form ordered films under ultrahigh vacuum conditions, presenting a well-contrasted diffraction pattern. Studies using high-resolution electron energy loss spectroscopy and ultraviolet photoelectron spectroscopy provide compelling evidence of a physisorbed system where the molecules only weakly interact with the substrate underneath. Comparisons with theoretical calculations, as well as with data obtained from optical spectroscopies, clearly demonstrate that the vibrational and electronic properties of the adsorbed molecules are similar to the expected ones for pristine pyrene. Finally, we used temperature-programmed X-rays photoelectron spectroscopy to study the desorption process of pyrene on the Ag(111) surface and estimate its activation energy to desorption.

INTRODUCTION

Polycyclic aromatic hydrocarbons (PAHs) correspond to organic compounds with two or more fused aromatic rings. They are among the most investigated and interesting molecules as their studies span from combustion and astrochemistry to nanotechnology or spintronics. PAHs are found to be abundant in interstellar space and represent a non-negligible part of the composition of the dust in the diffuse interstellar medium.[1−4] They thus play an important role in the chemistry of space, and their contribution to the formation of H_2, the most abundant molecule in space, has been extensively investigated.[4−7] It is therefore of particular interest to carry out fundamental studies on such molecules as well as their derivatives, from both a chemical and physical point of view, to determine their reactivity with surfaces and their behavior under various conditions such as X-rays or ultraviolet (UV) irradiations and oxidation or hydrogenation.[8−13]

On the other hand, hybrid interfaces between conjugated organic molecules and metals constitute an intensive and vast field of research and are of great importance for the performance of organic-based devices in organic electronics, more particularly, the first interface between an organic monolayer and a conductive electrode, which is crucial for charge injection and thus device efficiency.[14−16] In this context, PAHs represent profuse case-school molecules because of their length, geometry, and reactivity with respect to the substrate underneath. More recently, in the blooming field of on-surface synthesis, the adsorption of neutral PAHs, and their derivatives, is studied as prototypical cases of organic precursors with the aim to form new architectures with specific dimensions and geometry, as in the case of the formation of graphene and graphene-derivated structures.[17−19] It has been shown that the chemistry and reactivity of PAHs are of valuable interest for the synthesis of graphene sheets of nanoribbons, which is of particular concern for nanoelectronics and spintronics.[20,21]

Finally, PAHs, and more particularly PAHs adsorbed on relatively inert substrates, constitute template molecules or systems for the development of theoretical calculations and more especially in the framework of van der Waals density functional theory (DFT).[22−25]

From the above reasons, it appears clearly that understanding the reactivity of PAHs and their derivatives, as well as their on-surface behavior, is of particular importance due to

Received: February 15, 2021
Revised: May 4, 2021
Published: May 18, 2021

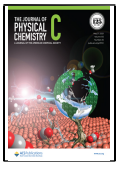

https://doi.org/10.1021/acs.jpcc.1c01350
J. Phys. Chem. C 2021, 125, 11166−11174

their potential implications in astrochemistry, nanoelectronics, and fundamental sciences.[26−28]

The presented work reports the study of the adsorption of pyrene molecules ($C_{16}H_{10}$), one of the smallest PAHs, on a Ag(111) surface, combining several surface-sensitive techniques. We demonstrate that pyrene molecules weakly interact with the Ag underneath, allowing us to determine some of their characteristic parameters such as their vibrational properties, ionization energy, and energy of activation to desorption.

METHODS

Most experiments presented in this work were conducted in a series of interconnected ultrahigh vacuum (UHV) chambers equipped with standard surface preparation facilities, a low-energy electron diffraction (LEED) apparatus, a scanning tunneling microscope, X-rays and ultraviolet photoelectrons spectroscopy facilities, as well as a high-resolution electron energy loss spectroscopy (HREELS) analysis. Additional experiments using optical techniques were carried out under atmospheric pressure.

The Ag(111) single-crystal surface, from Surface Preparation Laboratory, was cleaned by several cycles of Ar^+ bombardment at 1500 eV, followed by annealing at around 700 K.

Pyrene molecules were provided by Sigma-Aldrich. They were evaporated from a well-outgassed quartz-crucible onto an atomically clean substrate held at room-temperature (RT). The coverage of the organic layer was estimated to be around 0.4 monolayer from the attenuation of the Ag 3d core levels, assuming a homogeneous film.

HREELS measurements were carried out using a VSI delta 0.5 spectrometer. Unless mentioned, all spectra were recorded with the same incident electron beam energy of 4 eV and with a typical energetic resolution of about 5 meV, estimated from the full width at half-maximum (FWHM) of the elastic peak. Scattering geometry: $\theta_i = \theta_s = 67°$ for specular geometry, $\theta_i = 67°$ and $\theta_s = 53°$ for off-specular conditions.

Ultraviolet photoemission spectroscopy (UPS) measurements were performed using He I ($h\nu$ = 21.22 eV) and He II ($h\nu$ = 40.81 eV) radiation from a HIS13 discharge lamp from Scienta Omicron. X-ray photoelectron spectroscopy (XPS) was carried out with the non-monochromatized Mg Kα line ($h\nu$ = 1254.6 eV) of an X-ray tube. The emitted photoelectrons were counted using an R3000 analyzer equipped with a microchannel plate detector. To measure the onset of photoemission, or cut-off of the secondary emission peak, and determine the work function (W.F.) of the surface, UPS spectra were collected while biasing the sample at −3 V. The resolution in UPS measurements, determined from the width of the Fermi step on the metallic substrates, was 0.15 eV. The resolution in XPS measurements, determined from the FWHM of Ag 3d core levels, recorded on the clean surface, was 0.8 eV.

Ultraviolet−visible (UV−vis) data were obtained in cyclohexane with a concentration of 1 μmol·L^{-1} and measured using an Agilent Cary 60 UV−vis spectrophotometer in the range from 210 to 415 nm with a typical resolution of 4 nm.

Infrared measurements were recorded from 600 to 4000 cm^{-1} using a Bruker IFS 66/S Fourier transform infrared spectrometer equipped with a HgCdTe detector. The data were recorded on pyrene powder, in attenuated total reflection (ATR) mode, using a Ge module and a typical resolution of 1 cm^{-1}.

DFT calculations on isolated pyrene were carried out to support experimental data. The geometric and vibrational structures were evaluated using the B3LYP hybrid functional and the 6-311++g(2d,2p) basis set implemented in Gaussian 16 package.[29] To compare the experimental data, a scaling factor of 0.955 and a rigid shift of −20 cm^{-1} were applied to the vibrational frequencies obtained from DFT calculations.

RESULTS AND DISCUSSION

Due to its high vapor pressure and weak intermolecular interaction, the growth of pyrene molecules (Figure 1) on RT crystal surfaces under UHV conditions is a challenging task.[30] Nevertheless, we managed to grow a film of pyrene exhibiting a well-defined LEED pattern as depicted in Figure 2.

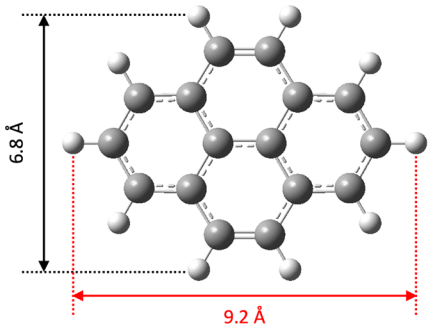

Figure 1. Schematic representation of a pyrene molecule.

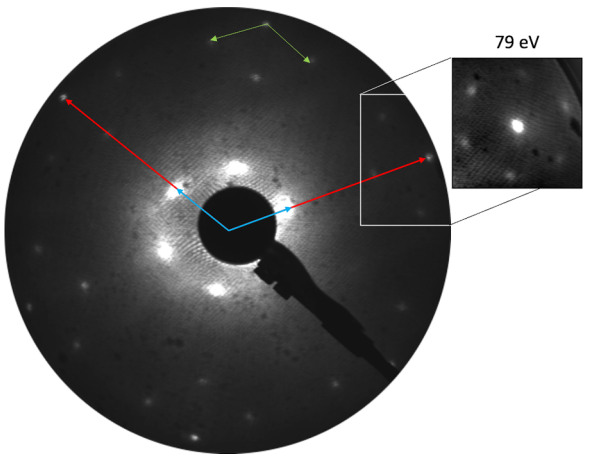

Figure 2. LEED pattern recorded at 50 eV. Red and blue arrows represent the unit vectors of the Ag surface and pyrene superstructure, respectively. Green arrows indicate the spots due to multiple diffractions. Top right inset represents the spot (1,0) recorded at 79 eV.

In this image, one can clearly observe that each diffraction spot of the Ag(111) surface is surrounded by six additional spots coming from the superstructure formed by the pyrene molecules. Careful spot analysis demonstrates that the lattice parameter of the unit cell adopted by the organic compound is about 3.4 times larger than the surface lattice parameter of the Ag(111) substrate. This corresponds to a closest neighbor distance of about 9.8 Å, a value which is, considering the steric hindrance of the system, consistent with the size of the pyrene molecule whose length is about 9.2 Å. However, the distance between two successive diffraction spots along one high

https://doi.org/10.1021/acs.jpcc.1c01350
J. Phys. Chem. C 2021, 125, 11166−11174

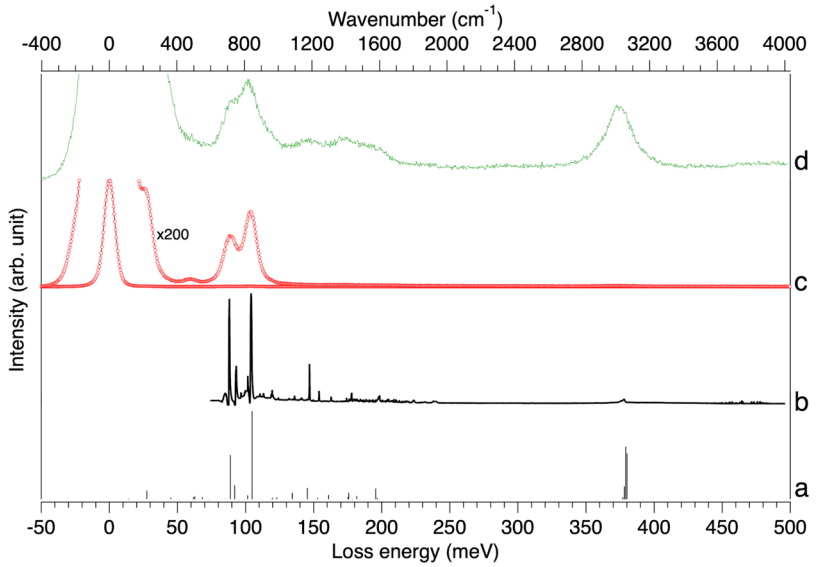

Figure 3. (a) Vertical sticks represent the theoretical vibrational modes of pyrene. (b) Full-line curve represents the ATR−FTIR measurement of pyrene powder. (c) Open-circle and (d) dashed-line spectra correspond to HREELS data of pyrene/Ag(111), recorded at 4 eV of primary energy, in specular and off-specular geometry, respectively.

symmetry direction is not equal. The mismatching, of about 35%, is too high to be attributed to a simple deformation of the image due to the projection of the Ewald sphere on a flat screen. To explain the observed LEED pattern, one has to consider that only the first-order diffraction spots, corresponding to the incommensurate matrix 1, are visible. This phenomenon can be explained by the fact that molecules, which weakly interact with each other, are highly mobile on the surface and thus form well-oriented domains of irregular width, preventing the observation of high-order diffraction spots, as in the case of rare gases adsorbed on surfaces, when the LEED pattern is recorded at high temperature or when domains of irregular widths are formed.[31−35] Unfortunately, we were not able to record any RT-scanning tunneling microscopy (STM) image of the adsorbed film possibly because of the high mobility of the molecules on the surface, supporting the aforementioned statements. In addition, let us mention that irregular arrangements of pyrene molecules on surfaces were already observed by low-temperature STM measurements.[30]

$$\begin{bmatrix} A \\ B \end{bmatrix} = \begin{bmatrix} 3.4 & 0 \\ 0 & 3.4 \end{bmatrix} \begin{bmatrix} i \\ j \end{bmatrix} \quad (1)$$

where A and B are the basis vectors of the molecular over-layer and i and j are those of Ag(111).

In order to characterize the adsorption of pyrene on Ag(111), we studied the system by means of HREELS and compared the obtained data with measurements collected by ATR−Fourier-transform infrared (FTIR) and UV−vis spectroscopy. Figure 3 shows the HREELS data together with ATR−FTIR spectrum as well as the infrared active vibrational modes obtained by DFT calculations.

On the HREELS data recorded in specular geometry, we observed, besides the elastic peak centered at 0 meV, four features located at 26 (210), 59 (476), 89 (718), and 104 (839) meV (cm^{-1}). Comparison with the infrared as well as the theoretical data allow us to conclude that these modes are characteristic of pristine pyrene. They can be respectively attributed to out-of-plane deformation of the macrocycle for the two lowest ones and out-of-plane bending modes of the C−H bonds for the two highest losses. Interestingly, around 375 meV (3025 cm^{-1}), a region corresponding to the C−H stretching modes of the molecule, no peak was perceived in specular conditions, while a clear component can be observed in off-specular geometry. Considering that in off-specular conditions the impact scattering regime is dominating as compared to the dipolar scattering regime governing the interaction in specular geometry, we could deduce that in the latter case, the created active dipole is no longer active because of its screening image in the metallic surface.[36] We could thus conclude that the molecules are adsorbed with their macrocycle parallel to the surface plane.

A tentative model, deduced from the LEED and HREELS measurements, of the adsorption of the pyrene molecules on the substrate is proposed in Figure 4. In the image, the red and blue arrows, respectively, represent the basis vectors of the Ag(111) and pyrene superstructure unit cells, in the real space. Since no image of the surface was obtained by STM, the azimuthal orientation of the molecules and their respective position with the Ag atoms underneath have been arbitrarily attributed.

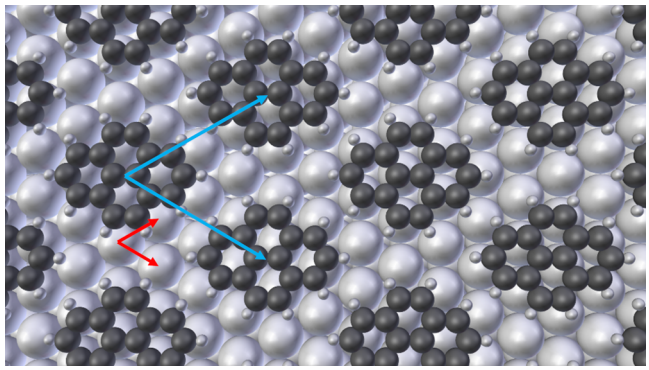

Figure 4. Graphical representation of a tentative adsorption model of pyrene molecules on a Ag(111) surface. The red and blue arrows, respectively, represent basis vectors of the Ag(111) and the molecular superstructure.

https://doi.org/10.1021/acs.jpcc.1c01350
J. Phys. Chem. C 2021, 125, 11166−11174

Looking now at higher energy losses, one could access information related to the electronic excitations, such as transitions between occupied and unoccupied electronic states. Figure 5 displays the HREELS spectra, recorded in specular

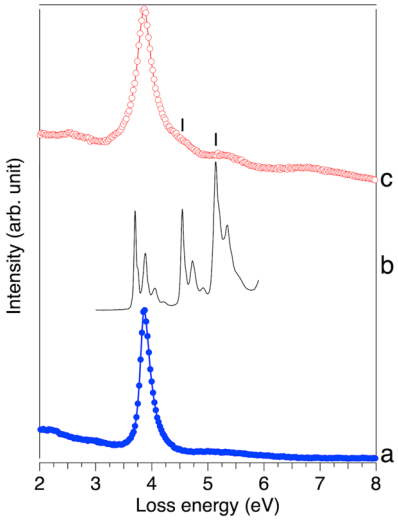

Figure 5. HREELS data recorded at 20 eV of primary energy, in specular condition, of the clean Ag(111) [full-circle curve, (a)] and pyrene on Ag(111) [open-circle curve, (c)] together with data obtained by UV−vis absorption spectroscopy of pyrene in cyclohexane [full-line curve, (b)]. The vertical ticks indicate the position of some features further discussed in the article.

geometry with a primary kinetic energy of 20 eV, of the clean Ag(111) and pyrene adsorbed on Ag(111) and the UV−vis spectrum of pyrene molecules dissolved in cyclohexane solution. The HREELS signal of pyrene on Ag(111) is dominated by an intense peak located at about 3.85 eV and corresponds to the excitation of the surface plasmon of Ag(111) as evidenced by the spectrum recorded on the clean surface. However, the spectrum measured after pyrene adsorption exhibits a softer slope of the left wing of the plasmon's peak and presents two additional shoulders around 4.5 and 5.2 eV. As indicated by the UV−vis spectrum of pyrene in solution, this is consistent with the position of the most intense absorption lines of pyrene observed in the UV−vis spectrum, as well as from pyrene in the gas phase.[37] The first of them, at about 3.8 eV, corresponds to the electronic transition between the highest occupied molecular orbital (HOMO) and the lowest unoccupied molecular orbital. This demonstrates again that the molecules remain in their pristine state after adsorption and thus they are only physisorbed on the surface. Let us also note that the loss spectrum exhibits a feature around 6.8 eV, corresponding to a high energetic transition not achievable by classical optical spectroscopy.

To further describe the adsorption of pyrene on the Ag(111) surface, we have undertaken photoemission spectroscopy measurements using a UV source. Figure 6 represents He I spectra showing the secondary electron cut-off (SECO) region as well as the valence band (VB) and the region close to the Fermi level.

From the onset observed in Figure 6a prior to adsorption, we could determine the work function of the clean Ag(111) at 4.54 ± 0.05 eV. After pyrene adsorption, the sample's work function decreases to 3.98 ± 0.05 eV. These work function values are deduced from the numerical difference between the

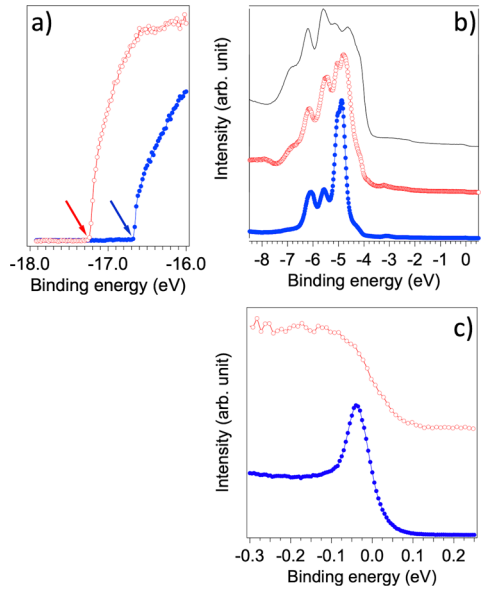

Figure 6. UPS spectra of pyrene on Ag(111) representing the (a) SECO region, (b) VB, and (c) region close to the Fermi level recorded using the He I emission line of the UV source, in normal emission. Open-circle and full-circle curves, respectively, correspond to pyrene/Ag(111) and clean Ag(111). Full-line curve on figure (b) corresponds to polycrystalline Ag. The arrows on figure (a) show the position of the onset of the SECO.

photon energy and the absolute value of the binding energy (BE) at which the onset of the SECO appears. Such decrease of the work function after adsorption of an organic compound on a surface is a well-known effect, named "Pillow-effect", and is due to the repealing of the metal electronic tail because of the presence of adsorbed molecules and yield to a potential drop at the interface. Such phenomenon is characteristic of physisorbed systems and has been thoroughly described in the literature.[38−42] Figure 6b represents the evolution of the Ag 4d levels prior and after adsorption together with the Ag 4d levels of a clean amorphous Ag using the He I line of the UV source. Before pyrene evaporation, the UPS spectrum mainly exhibits four components of which the two lowest BE ones (at −5 eV) are much more intense than the two highest BE ones (around −5.5 and −6 eV). Subsequently to pyrene deposition, the overall shape of the Ag 4d is changed. First of all, the ratio between the two lowest BE components and the two highest BE ones is strongly modified. In addition, a new feature revealed by a shoulder around −6.8 eV appears. A first guess would be thinking that this new electronic structure could be attributed to the electronic level of the pyrene molecules. However, comparing the spectrum of the Ag 4d of the Ag(111) after adsorption with the one of a clean polycrystalline Ag, the aforementioned hypothesis is not that straightforward. Indeed, the VB of clean polycrystalline Ag also presents shoulders around −6.8 eV. It is known that the interpretation of UPS spectra can be misleading because of photoelectron diffraction effects at the organic−inorganic interfaces. Indeed, interface scattering of substrate photoelectrons from the bulk, like surface-umklapp process or backfolding of substrate bands, may affect the energy distribution curves when organic molecules are adsorbed on single-crystal surfaces of noble metals. In the case of Ag(111), it has been already demonstrated that the Ag 4d spectrum becomes close to that of a polycrystalline sample upon adsorption of large π-

https://doi.org/10.1021/acs.jpcc.1c01350
J. Phys. Chem. C 2021, 125, 11166−11174

conjugated molecules.[43] Thus, photoelectron diffraction effect is most probably at the origin of the modification of the intensity ratio of the Ag 4d spectrum. In contrast to the adsorption of zinc phthalocyanine on Ag(111), the closeness of the Ag 4d spectrum of pyrene on Ag(111) with the one of polycrystalline Ag is less clear. This is likely due to the fact that pyrene molecules do not form long-range order superstructures and that they are highly mobile on the surface. Therefore, the observed spectrum of the Ag 4d is somewhere in between that of the clean Ag(111) and the clean polycrystalline. Considering this point, it is difficult to attribute the physical origin of the shoulder at −6.8 eV. It can either be due to the presence of some density of states (DOS) of the molecules as well as to some photoelectron diffraction effects since a shoulder is also observed in this region in the case of polycrystalline Ag or both. Concerning the component at −7.9 eV, it cannot be explained by the diffraction effect, as it is not present on the polycrystalline Ag spectrum, and thus attributed to an occupied molecular orbital of the pyrene molecules. Finally, some structures located at −3 eV BE can be observed on all spectra. In our case, considering that our UV source is not monochromatized, as well as the intensity ratio between these features and the Ag VB, we can mainly attribute these components to the signal from the Ag 4d levels excited by the satellite lines (referred to as He I − β and He I − γ) of the main He I line (He I − α). Since in the case of pyrene on Ag(111), this peak can also be due to some molecular DOS and further description of this region will be given using the He II line, as described below. Nevertheless, the effect of these satellite lines does not affect the close vicinity of the Fermi level (E_F). As depicted in Figure 6c, on the clean Ag(111), a clear peak, attributed to the Ag(111) surface-state, is observed close to E_F, while it is no longer the case after adsorption of pyrene, as in the case of a rare gas or molecules adsorbed on Ag(111) and other noble metals.[44−50] This can actually be explained in terms of an energetic shift toward lower BE that is, closer to the E_F, of the surface-state caused by Pauli repulsion between the π-electrons of the molecules and the Shockley-state wave function out of the crystal. In the case of Ag(111), since the surface-state is already very close to the Fermi level, it even shifts above it, becoming completely unoccupied and thus not observable by UPS.

As mentioned earlier, since our UV source is not monochromatic, the inspection of the VB at about 2−4 eV from the Fermi level using the He I line is not suitable because of the contribution of the satellite lines. Therefore, to provide a cautious determination of the electronic properties of pyrene molecules on Ag(111), we have undertaken similar measurements using the He II line. Moreover, using He II allows much more surface sensitivity, thus limiting the side effects due to photoelectron diffraction at the interface. Figure 7a represents the UPS spectrum in the same BE range as the one taken using He I, and Figure 7b corresponds to a zoom-in of the region close to the Fermi level.

After pyrene evaporation, the spectrum exhibits new features around −7.9, −3.3, and −2.5 eV from the Fermi level, together with a reinforcement of the shoulder at −6.8 eV. The two highest BE features at −7.9 and −6.8 eV, already measured using He I, can thus be attributed to molecular electronic levels and no longer to the photoelectron diffraction effect. The two structures detected close to the Fermi level, that were not clearly revealed using He I because of the satellite lines, can now be seen as representative of the electronic properties of

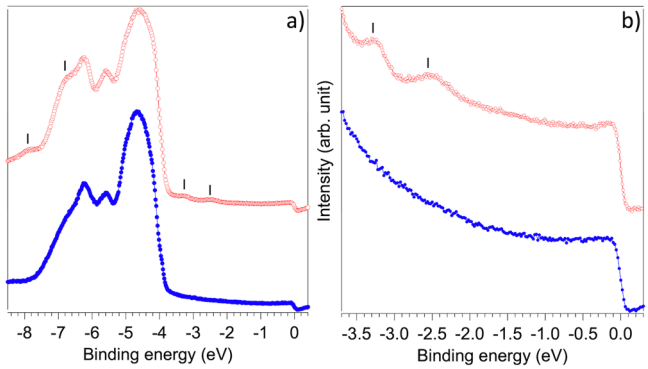

Figure 7. UPS spectra of pyrene on Ag(111) representing the (a) VB and (b) region close to the Fermi level recorded using the He II emission line of the UV source, in normal emission. Open-and full-circle curves, respectively, correspond to pyrene/Ag(111) and clean Ag(111). The vertical ticks indicate the position of some features further discussed in the article.

the molecules. To have a better picture of the DOS of pyrene, we display, in Figure 8, a comparison between the theoretical

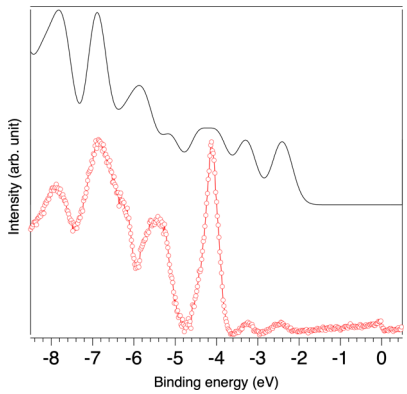

Figure 8. Comparison between the DOS obtained from DFT calculations (full-line) with the experimental DOS (open-circle curve) extracted by subtracting the contribution of the clean silver to the VB spectrum of pyrene/Ag(111) using the He II emission line.

calculation and experimental data obtained by subtracting the spectrum of the clean Ag(111) from the one recorded after adsorption using the He II emission line.

The overall position of the calculated peaks match fairly well the theoretical ones, demonstrating once more that pyrene molecules are still in their pristine state even after adsorption, confirming that they poorly interact with the surface underneath, as expected from a physisorbed system. From the onset on the lowest BE feature, situated about −2.1 eV from the Fermi level, we have estimated the value of the ionization energy (I.E.) of the pyrene molecules to be around 6.1 ± 0.1 eV (I.E. = $W.F._{sample}$ + $|HOMO_{onset}|$). This value is, as expected, smaller than the value of the ionization energy measured in the gas phase, that is, around 7.4 eV as measured by photoemission, and consistent with the value of 5.8 eV obtained in a condensed phase.[51−54] The energy difference between the values obtained in gas and solid phases arises from polarization effects due to different screening of the existing charges created by the surrounding medium during the photoemission process.[55−57] In our case, the polarization energy, obtained from the difference between the I.E. of pyrene

https://doi.org/10.1021/acs.jpcc.1c01350
J. Phys. Chem. C 2021, 125, 11166−11174

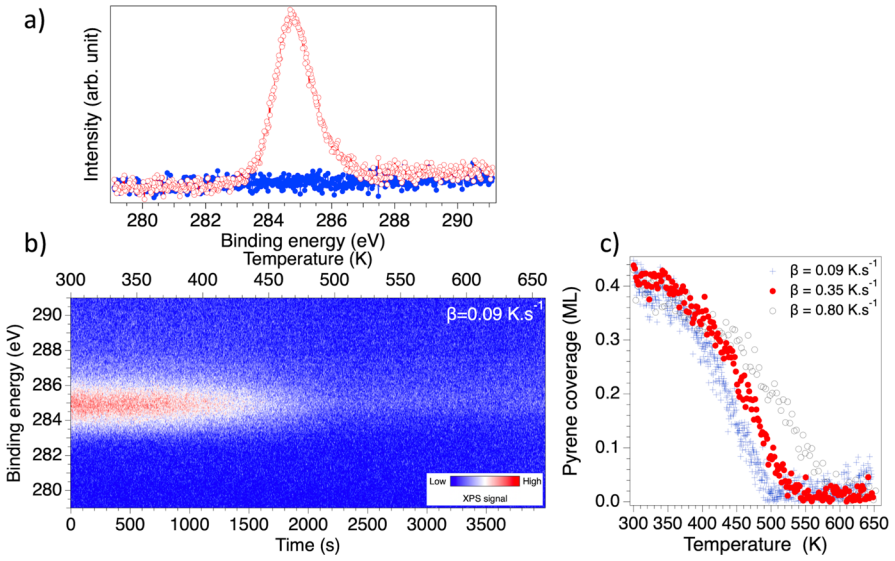

Figure 9. (a) C 1s core level region/red open-circle and blue closed-circle curves, respectively, correspond to pyrene/Ag(111) and clean Ag(111). (b) 2D map representing the evolution of the C 1s of the pyrene as a function of time and annealing temperature. (c) Integrated C 1s signal as a function of the temperature.

in the gas phase and its I.E. measured in this work, is about 1.3 eV ± 0.1 eV, a value which is consistent but slightly below the value of 1.6 eV reported by Sato and co-workers as well as with the common value of 1.7 eV reported for most of the planar PAHs in the condensed phase.[54] The fact that we got a smaller polarization energy value is most probably related to the small molecular density on the Ag(111) surface, as compared to denser organic solids.

Finally, using temperature-programmed XPS (TP-XPS), we studied the desorption of pyrene on Ag(111) upon annealing. With such an aim, we have recorded the evolution of the C 1s core level of the pyrene molecules as a function of the sample temperature from RT up to 650 K using three different linear ramps of 0.09, 0.35, and 0.8 $K{\cdot}s^{-1}$. Figure 9a represents the C 1s core level region prior to and after adsorption. Figure 9b displays a 2D map representing the evolution of the C 1s spectrum region as a function of the sample temperature. In the image, it can be observed that the amplitude of the C 1s signal decreased as the temperature increased. This behavior is properly illustrated in Figure 9c.

With the aim to interpret the TP-XPS data and to determine the desorption parameters, that is, the activation energy and pre-exponential frequency factor, we used the following Polanyi–Wigner equation, commonly employed to describe the desorption of adsorbates from surfaces[58,59]

$$\frac{d\Theta}{dt} = -\nu{\cdot}\Theta^{n}{\cdot}\exp\left(\frac{-E_a}{k_B{\cdot}(T_0 + \beta{\cdot}t)}\right) \quad (2)$$

where Θ represents the instantaneous pyrene coverage, ν is the pre-exponential frequency factor, E_a is the activation energy to desorption, T_0 is the initial temperature set at RT, β is the linear heating ramp, and n is the order of the desorption kinetics, set to 1, considering the weak intermolecular interactions, the weak molecule–substrate interactions, and the relatively low molecular density.

It is not trivial and straightforward to have a good estimation of both the activation energy to desorption and the pre-exponential frequency factor, for which several papers have shown that it depends on the adsorbate and can vary over several orders of magnitude.[60−65] Therefore, we decide to present and discuss different results using two different values of ν.

We have first simply interpreted the pre-exponential factor as a typical surface phonon frequency, which corresponds to a value in the range of 10^{13} s^{-1}. Such a value is the "typical" frequency factor used in thermal desorption experiments for atoms and small molecules but also for tetracene and pentacene, which are two PAHs relatively close to pyrene in terms of the number of benzene rings.[61,63,66−68] It was also used by Günther *et al.* for an even larger molecule.[69] Then, we have exploited a value of $\nu = 5.5 \times 10^{18}$ s^{-1} obtained from the transition state theory (TST) that considers changes in the entropy going from adsorbed to transition states.[64,70,71] The description of the determination of the pre-exponential factor using the TST is given in the Supporting Information.

A first-kinetics desorption model using the aforementioned Polanyi–Wigner equation and pre-exponential frequency factors allows us to obtain two different values of the activation energy to desorption, summarized in Table 1.

Table 1. Activation Energy to Desorption (E_a) Extracted from the Fitting Procedure as a Function of the Pre-exponential Frequency Faction (ν), Together with the Energy per Carbon Atom

ν (s^{-1})	E_a (eV)	E_a ($kJ{\cdot}mol^{-1}$)	energy per C atom (meV)
1×10^{13}	1.38 ± 0.04	133 ± 4	86
5.5×10^{18}	1.90 ± 0.10	184 ± 10	119

Let us first note that the value obtained using the lowest frequency factor is consistent with the value obtained for tetracene and pentacene on Ag(111) using a similar frequency factor and agrees with the theoretical values from Björk *et al.* on graphene.[18,66,68] If the similarity between the adsorption energy for these three molecules on Ag(111) is not surprising given their closeness, the fact that they also agree on the data on graphene is more questionable. Indeed, graphene and its derivative highly oriented pyrolytic graphite (HOPG) are

https://doi.org/10.1021/acs.jpcc.1c01350
J. Phys. Chem. C 2021, 125, 11166−11174

known to be relatively inert with respect to organic molecules, while it has been shown that Ag(111) can be more reactive, even with PAHs, involving charge transfer between the molecules and the substrate.[23,72,73] Thus, one might expect a higher desorption energy value, at least at monolayer coverage, as in the work of Tao *et al.* for tetracene on Ag(110), in which they obtained a theoretical adsorption energy value of about 2.05 ± 0.25 eV.[74] Also, a recent work from Morbec and Kratzer, including van der Waals (vdW) interactions in their DFT calculations of pentacene on Ag(111), found, for flat-lying molecules, an average value of the adsorption energy of about 2.2 eV,[24] a value much higher than the one obtained considering the pre-exponential factor in the 10^{13} s^{-1} range. Interestingly, for the latter system, Kafer *et al.* have experimentally determined an activation energy to desorption of 2.14 eV by thermal desorption spectroscopy but using a pre-exponential factor of 1.6×10^{19} s^{-1}, a value quite close to the one obtained using the TST ($\sim 2 \times 10^{19}$ s^{-1}).[73,75] This value of the energy to desorption is actually in good agreement with previous values of pentacene adsorbed on Au and Cu substrates.[76] This actually demonstrates that for large molecules restricting the pre-exponential factor to the typical surface phonon frequency is probably not correct and leads to underestimated values of the adsorption energy. Hence, we performed a similar analysis of our experimental data using the value of the frequency factor obtained from the TST ($\nu = 5.5 \times 10^{18}$ s^{-1}). This yields an activation energy to desorption of 1.9 eV, corresponding to an energy per carbon atom of about 119 meV. Unsurprisingly, this value is much higher than the previous one and those from the literature for PAHs of similar size[18,59,77] adsorbed on graphene of HOPG. They are mainly two reasons for such a difference. On the one hand, and as discussed before, Ag(111) is known to be more reactive than graphene and its derivatives and thus its interaction with PAHs is higher than that of graphene-based substrates. On the other hand, most of the values reported in the literature have been obtained using lower frequency factors, undeniably leading to lower desorption energies. Let us note that our finding is consistent with the value obtained by Kafer for pentacene of Ag(111)[75] when using a frequency factor similar to the one obtained from TST. In the light of the work of Morbec and Kratzer, we demonstrate here that even if only weak molecules−substrate interactions, such as van der Waals type interactions, are involved, while they do not modify the vibrational nor the electronic properties of the adsorbed molecules with respect to their pristine state, they may have important influence on the desorption energy, especially for flat-lying molecules.[24] Thus, even if we cannot compare the desorption values obtained by TP-XPS with other experimental or theoretical data, we suggest that in the case of large molecules, adsorbed on surfaces, up to the monolayer coverage, the most rigorous way to determine their desorption energy is to use a pre-exponential frequency factor derived from the TST.

CONCLUSIONS

In summary, we have studied the adsorption, under UHV conditions and at RT, of pyrene molecules on a Ag(111) single-crystal, combining various surface-sensitive techniques. We demonstrated that even if this represents a challenging task because of the relatively high vapor pressure of pyrene, the molecules can form a superstructure of small size presenting a 3.4 times periodicity with the substrate underneath. As expected, molecules weakly interact with the substrate and both their vibrational and electronic properties are similar to those of pristine molecules. Finally, we have estimated the activation energy to desorption of pyrene on Ag(111) from temperature-programmed XPS measurements following the evolution of the C 1s component as a function of the sample temperature. A comparison with a first-kinetics order desorption model allowed us to determine its value around 1.9 eV (184 $kJ \cdot mol^{-1}$).

ASSOCIATED CONTENT

Supporting Information

The Supporting Information is available free of charge at https://pubs.acs.org/doi/10.1021/acs.jpcc.1c01350.

Estimation of the pre-exponential frequency factor using the transition state theory (ZIP)

Brief explanation of the estimation of the pre-exponential frequency factor using the TST (PDF)

AUTHOR INFORMATION

Corresponding Author

Eric Salomon − *Aix-Marseille University, CNRS, PIIM, 13013 Marseille, France;* orcid.org/0000-0002-0567-7438; Email: eric.salomon@univ-amu.fr

Authors

Marco Minissale − *Aix-Marseille University, CNRS, PIIM, 13013 Marseille, France*

Francisco Romero Lairado − *Aix-Marseille University, CNRS, PIIM, 13013 Marseille, France*

Stephane Coussan − *Aix-Marseille University, CNRS, PIIM, 13013 Marseille, France;* orcid.org/0000-0002-0275-7272

Pierre Rousselot-Pailley − *Aix-Marseille University, Centrale Marseille, CNRS, iSm2, 13013 Marseille, France;* orcid.org/0000-0002-7658-9056

François Dulieu − *CY Cergy Paris Université, Sorbonne Université, Observatoire de Paris, PSL University, CNRS, LERMA, F-95000 Cergy, France*

Thierry Angot − *Aix-Marseille University, CNRS, PIIM, 13013 Marseille, France*

Complete contact information is available at: https://pubs.acs.org/10.1021/acs.jpcc.1c01350

Notes

The authors declare no competing financial interest.

ACKNOWLEDGMENTS

The authors thank the financial support from the French National Research Agency under the project "DUALITY" (project no ANR-17-CE08-0010). The financial support from the council of the Sud region of France, under the project "POLYPHENE" is also gratefully acknowledged.

REFERENCES

(1) Tielens, A. G. G. M.; Allamandola, L. J.; Hollenbach, D.; Thronson, H. Interstellar processes. In *Proceedings of the Symposium*, Grand Teton National Park, WY. Dordrecht, D, Reidel Publishing Co., 1987, p 397.

(2) Tielens, A. G. G. M. Interstellar Polycyclic Aromatic Hydrocarbon Molecules. *Annu. Rev. Astron. Astrophys.* **2008**, *46*, 289−337.

(3) Allamandola, L. J.; Sandford, S. A.; Wopenka, B. Interstellar Polycyclic Aromatic Hydrocarbons and Carbon in Interplanetary Dust Particles and Meteorites. *Science* **1987**, *237*, 56−59.
(4) Campisi, D.; Simonsen, F. D. S.; Thrower, J. D.; Jaganathan, R.; Hornekær, L.; Martinazzo, R.; Tielens, A. G. G. M. Superhydrogenation of pentacene: the reactivity of zigzag-edges. *Phys. Chem. Chem. Phys.* **2020**, *22*, 1557−1565.
(5) Bauschlicher, C. W., Jr. The Reaction of Polycyclic Aromatic Hydrocarbon Cations with Hydrogen Atoms: The Astrophysical Implications. *Astrophys. J.* **1998**, *509*, L125−L127.
(6) Rauls, E.; Hornekær, L. Catalyzed Routes to Molecular Hydrogen Formation and Hydrogen Addition Reactions on Neutral Polycyclic Aromatic Hydrocarbons under Interstellar Conditions. *Astrophys. J.* **2008**, *679*, 531−536.
(7) Thrower, J. D.; Jørgensen, B.; Friis, E. E.; Baouche, S.; Mennella, V.; Luntz, A. C.; Andersen, M.; Hammer, B.; Hornekær, L. Experimental Evidence for the Formation of Highly Superhydrogenated Polycyclic Aromatic Hydrocarbons through H Atom Addition and Their Catalytic Role in H2Formation. *Astrophys. J.* **2012**, *752*, 3.
(8) Jochims, H. W.; Ruhl, E.; Baumgartel, H.; Tobita, S.; Leach, S. Size Effects on Dissociation Rates of Polycyclic Aromatic Hydrocarbon Cations: Laboratory Studies and Astrophysical Implications. *Astrophys. J.* **1994**, *420*, 307.
(9) Panchagnula, S.; Bouwman, J.; Rap, D. B.; Castellanos, P.; Candian, A.; Mackie, C.; Banhatti, S.; Brünken, S.; Linnartz, H.; Tielens, A. G. G. M. Structural investigation of doubly-dehydrogenated pyrene cations. *Phys. Chem. Chem. Phys.* **2020**, *22*, 21651−21663.
(10) Zhen, J.; Yang, Y.; Zhang, W.; Zhu, Q. Formation and photochemistry of covalently bonded large functional PAH clusters. *Astron. Astrophys.* **2019**, *628*, A57.
(11) Dulieu, F.; Morisset, S.; Ibrahim Mohamed, A.-S.; Boshman, L.; Cazaux, S.; Teillet-Billy, D.; Baouche, S.; Rougeau, N. Reactivity of coronene with O-atoms, a possible route to ketene in the interstellar medium. *Mol. Astrophys.* **2019**, *17*, 100054.
(12) Joblin, C.; Wenzel, G.; Castillo, S. R.; Simon, A.; Sabbah, H.; Bonnamy, A.; Toublanc, D.; Mulas, G.; Ji, M.; Giuliani, A.; et al. Photo-processing of astro-PAHs. *J. Phys. Conf.* **2020**, *1412*, 062002.
(13) Singh, S.; Gupta, D.; Antony, B.; Tudorovskaya, M.; Tennyson, J. Electron Scattering Cross Sections for Anthracene and Pyrene. *J. Phys. Chem. A* **2020**, *124*, 7088−7100.
(14) Ishii, H.; Sugiyama, K.; Ito, E.; Seki, K. Energy Level Alignment and Interfacial Electronic Structures at Organic/Metal and Organic/Organic Interfaces. *Adv. Mater.* **1999**, *11*, 605−625.
(15) Koch, N. Organic Electronic Devices and Their Functional Interfaces. *ChemPhysChem* **2007**, *8*, 1438−1455.
(16) Salomon, E.; Beato-Medina, D.; Verdini, A.; Cossaro, A.; Cvetko, D.; Kladnik, G.; Floreano, L.; Angot, T. Correlation between Charge Transfer and Adsorption Site in CoPc Overlayers Adsorbed on Ag(100). *J. Phys. Chem. C* **2015**, *119*, 23422−23429.
(17) Müllen, K.; Rabe, J. P. Nanographenes as Active Components of Single-Molecule Electronics and How a Scanning Tunneling Microscope Puts Them To Work. *Acc. Chem. Res.* **2008**, *41*, 511−520.
(18) Björk, J.; Hanke, F.; Palma, C.-A.; Samori, P.; Cecchini, M.; Persson, M. Adsorption of Aromatic and Anti-Aromatic Systems on Graphene through pi-pi Stacking. *J. Phys. Chem. Lett.* **2010**, *1*, 3407−3412.
(19) Narita, A.; Wang, X.-Y.; Feng, X.; Müllen, K. New advances in nanographene chemistry. *Chem. Soc. Rev.* **2015**, *44*, 6616−6643.
(20) Raman, K. V.; Kamerbeek, A. M.; Mukherjee, A.; Atodiresei, N.; Sen, T. K.; Lazić, P.; Caciuc, V.; Michel, R.; Stalke, D.; Mandal, S. K.; et al. Interface-engineered templates for molecular spin memory devices. *Nature* **2013**, *493*, 509−513.
(21) Weippert, J.; Hauns, J.; Bachmann, J.; Greisch, J.-F.; Narita, A.; Müllen, K.; Böttcher, A.; Kappes, M. M. Oligomerization of Dehydrogenated Polycyclic Aromatic Hydrocarbons on Highly Oriented Pyrolytic Graphite. *J. Phys. Chem. C* **2020**, *124*, 8236−8246.
(22) Chakarova-Käck, S. D.; Schröder, E.; Lundqvist, B. I.; Langreth, D. C. Application of van der Waals Density Functional to an Extended System: Adsorption of Benzene and Naphthalene on Graphite. *Phys. Rev. Lett.* **2006**, *96*, 146107.
(23) Toyoda, K.; Hamada, I.; Lee, K.; Yanagisawa, S.; Morikawa, Y. Density functional theoretical study of pentacene/noble metal interfaces with van der Waals corrections: Vacuum level shifts and electronic structures. *J. Chem. Phys.* **2010**, *132*, 134703.
(24) Morbec, J. M.; Kratzer, P. The role of the van der Waals interactions in the adsorption of anthracene and pentacene on the Ag(111) surface. *J. Chem. Phys.* **2017**, *146*, 034702.
(25) Chilukuri, B.; Mazur, U.; Hipps, K. W. Cooperativity and coverage dependent molecular desorption in self-assembled monolayers: computational case study with coronene on Au(111) and HOPG. *Phys. Chem. Chem. Phys.* **2019**, *21*, 10505−10513.
(26) Anthony, J. E. Functionalized Acenes and Heteroacenes for Organic Electronics. *Chem. Rev.* **2006**, *106*, 5028−5048.
(27) Fernández, I. Understanding the reactivity of polycyclic aromatic hydrocarbons and related compounds. *Chem. Sci.* **2020**, *11*, 3769−3779.
(28) Curcio, D.; Sierda, E.; Pozzo, M.; Bignardi, L.; Sbuelz, L.; Lacovig, P.; Lizzit, S.; Alfè, D.; Baraldi, A. Unusual reversibility in molecular break-up of PAHs: the case of pentacene dehydrogenation on Ir(111). *Chem. Sci.* **2021**, *12*, 170−178.
(29) Frisch, M. J.; Trucks, G. W.; Schlegel, H. B.; Scuseria, G. E.; Robb, M. A.; Cheeseman, J. R.; Scalmani, G.; Barone, V.; Petersson, G. A.; Nakatsuji, H. et al. *Gaussian 16*, Revision A.03; Gaussian Inc: Wallingford CT, 2016.
(30) Schleicher, S.; Borca, B.; Rawson, J.; Matthes, F.; Bürgler, D. E.; Kögerler, P.; Schneider, C. M. Ultra-High Vacuum Deposition of Pyrene Molecules on Metal Surfaces. *Phys. Status Solidi B* **2018**, *255*, 1800235.
(31) Boato, G.; Cantini, P.; Tatarek, R. Diffraction of He and H2molecular beams from a low temperature metal surface. *J. Phys. F: Met. Phys.* **1976**, *6*, L237−L240.
(32) Biberian, J.-P. Leed and Aes study of the Au/AuPb2 interface. *Surf. Sci.* **1978**, *74*, 437−460.
(33) Angot, T.; Suzanne, J. LEED studies of krypton and nitrogen monolayers on MgO(100) single crystals. *The Structure of Surfaces III*, **1990**.
(34) Hill, N. R.; Haller, V. Van der Waals forces and molecular diffraction from metal surfaces, with application to Ag(111). *Chem. Phys.* **1982**, *73*, 363−375.
(35) Zhachuk, R.; Coutinho, J.; Dolbak, A.; Cherepanov, V.; Voigtländer, B. Si(111) strained layers on Ge(111): Evidence for c(2×4) domains. *Phys. Rev. B* **2017**, *96*, 085401.
(36) Ibach, H.; Mills, D. *Electron Energy Loss Spectroscopy and Surface Vibrations*; Elsevier Science, 2013.
(37) Thöny, A.; Rossi, M. J. Gas-phase UV spectroscopy of anthracene, xanthone, pyrene, 1-bromopyrene and 1,2,4-trichlorobenzene at elevated temperatures. *J. Photochem. Photobiol., A* **1997**, *104*, 25−33.
(38) Vázquez, H.; Dappe, Y. J.; Ortega, J.; Flores, F. Energy level alignment at metal/organic semiconductor interfaces: "Pillow" effect, induced density of interface states, and charge neutrality level. *J. Chem. Phys.* **2007**, *126*, 144703.
(39) Vázquez, H.; Dappe, Y. J.; Ortega, J.; Flores, F. A unified model for metal/organic interfaces: IDIS, 'pillow' effect and molecular permanent dipoles. *Appl. Sci.* **2007**, *254*, 378−382.
(40) Hwang, J.; Wan, A.; Kahn, A. Energetics of metal−organic interfaces: New experiments and assessment of the field. *Mater. Sci. Eng., R* **2009**, *64*, 1−31.
(41) Flores, F.; Ortega, J. *The Molecule−Metal Interface*; John Wiley and Sons, Ltd, 2013; Chapter 2, pp 15−49.
(42) Kahn, A. Fermi level, work function and vacuum level. *Mater. Horiz.* **2016**, *3*, 7−10.
(43) Giovanelli, L.; Bocquet, F. C.; Amsalem, P.; Lee, H.-L.; Abel, M.; Clair, S.; Koudia, M.; Faury, T.; Petaccia, L.; Topwal, D.; et al. Interpretation of valence band photoemission spectra at organic-metal

interfaces. *Phys. Rev. B: Condens. Matter Mater. Phys.* **2013**, *87*, 035413.
(44) Marks, M.; Zaitsev, N. L.; Schmidt, B.; Schwalb, C. H.; Schöll, A.; Nechaev, I. A.; Echenique, P. M.; Chulkov, E. V.; Höfer, U. Energy shift and wave function overlap of metal-organic interface states. *Phys. Rev. B: Condens. Matter Mater. Phys.* **2011**, *84*, 081301.
(45) Andreev, T.; Barke, I.; Hövel, H. Adsorbed rare-gas layers on Au(111): Shift of the Shockley surface state studied with ultraviolet photoelectron spectroscopy and scanning tunneling spectroscopy. *Phys. Rev. B: Condens. Matter Mater. Phys.* **2004**, *70*, 205426.
(46) Behm, R. J.; Brundle, C. R.; Wandelt, K. The underlayer influence on photoemission and thermal desorption of xenon adsorbed on Ag(111). *J. Chem. Phys.* **1986**, *85*, 1061−1073.
(47) Hövel, H.; Grimm, B.; Reihl, B. Modification of the Shockley-type surface state on Ag(111) by an adsorbed xenon layer. *Surf. Sci.* **2001**, *477*, 43−49.
(48) Kanai, K.; Ouchi, Y.; Seki, K. Modification of Shockley surface state by long-chain n-alkane: Photoemission study on tetratetracontane/Au(111) interface. *Thin Solid Films* **2009**, *517*, 3276−3280.
(49) Andrews, K. M.; Pearl, T. P. Modification of Ag(111) surface electronic structure via weak molecular adsorption of adenine measured with low temperature scanning tunneling microscopy and spectroscopy. *J. Chem. Phys.* **2010**, *132*, 214701.
(50) Forster, F.; Bendounan, A.; Ziroff, J.; Reinert, F. Importance of surface states on the adsorption properties of noble metal surfaces. *Phys. Rev. B: Condens. Matter Mater. Phys.* **2008**, *78*, 161408.
(51) Wacks, M. E. Electron-Impact Studies of Aromatic Hydrocarbons. II. Naphthacene, Naphthaphene, Chrysene, Triphenylene, and Pyrene. *J. Chem. Phys.* **1964**, *41*, 1661−1666.
(52) Becker, R. S.; Chen, E. Extension of Electron Affinities and Ionization Potentials of Aromatic Hydrocarbons. *J. Chem. Phys.* **1966**, *45*, 2403−2410.
(53) Boschi, R.; Schmidt, W. Photoelectron spectra of polycyclic aromatic hydrocarbons. Pyrene and coronene. *Tetrahedron Lett.* **1972**, *13*, 2577−2580.
(54) Sato, N.; Seki, K.; Inokuchi, H. Polarization energies of organic solids determined by ultraviolet photoelectron spectroscopy. *J. Chem. Soc., Faraday Trans. 2* **1981**, *77*, 1621−1633.
(55) Salaneck, W. R. Intermolecular Relaxation Energies in Anthracene. *Phys. Rev. Lett.* **1978**, *40*, 60−63.
(56) Amy, F.; Chan, C.; Kahn, A. Polarization at the gold/pentacene interface. *Org. Electron.* **2005**, *6*, 85−91.
(57) Sun, H.; Ryno, S.; Zhong, C.; Ravva, M. K.; Sun, Z.; Körzdörfer, T.; Brédas, J.-L. Ionization Energies, Electron Affinities, and Polarization Energies of Organic Molecular Crystals: Quantitative Estimations from a Polarizable Continuum Model (PCM)-Tuned Range-Separated Density Functional Approach. *J. Chem. Theory Comput.* **2016**, *12*, 2906−2916.
(58) King, D. A. Thermal desorption from metal surfaces: A review. *Surf. Sci.* **1975**, *47*, 384−402.
(59) Zacharia, R.; Ulbricht, H.; Hertel, T. Interlayer cohesive energy of graphite from thermal desorption of polyaromatic hydrocarbons. *Phys. Rev. B: Condens. Matter Mater. Phys.* **2004**, *69*, 155406.
(60) Baetzold, R.; Somorjai, G. Preexponential factors in surface reactions. *J. Catal.* **1976**, *45*, 94−105.
(61) Tait, S. L.; Dohnálek, Z.; Campbell, C. T.; Kay, B. D. n-alkanes on MgO(100). II. Chain length dependence of kinetic desorption parameters for small n-alkanes. *J. Chem. Phys.* **2005**, *122*, 164708.
(62) Doronin, M.; Bertin, M.; Michaut, X.; Philippe, L.; Fillion, J.-H. Adsorption energies and prefactor determination for CH3OH adsorption on graphite. *J. Chem. Phys.* **2015**, *143*, 084703.
(63) Fichthorn, K. A.; Miron, R. A. Thermal Desorption of Large Molecules from Solid Surfaces. *Phys. Rev. Lett.* **2002**, *89*, 196103.
(64) Thrower, J. D.; Friis, E. E.; Skov, A. L.; Nilsson, L.; Andersen, M.; Ferrighi, L.; Jørgensen, B.; Baouche, S.; Balog, R.; Hammer, B.; et al. Interaction between Coronene and Graphite from Temperature-Programmed Desorption and DFT-vdW Calculations: Importance of Entropic Effects and Insights into Graphite Interlayer Binding. *J. Phys. Chem. C* **2013**, *117*, 13520−13529.
(65) Winkler, A. *Interface Controlled Organic Thin Films*; Al-Shamery, K., Horowitz, G., Sitter, H., Rubahn, H.-G., Eds.; Springer Berlin Heidelberg: Berlin, Heidelberg, 2009; pp 29−36.
(66) Gonella, G.; Dai, H.-L.; Rockey, T. J. Tetracene Monolayer and Multilayer Thin Films on Ag(111): Substrate-Adsorbate Charge-Transfer Bonding and Inter-Adsorbate Interaction. *J. Phys. Chem. C* **2008**, *112*, 4696−4703.
(67) Rockey, T. J.; Wilhelm, M. J.; Dai, H.-L. *Ultrathin Films of Pentacene on Ag(111): Charge-Transfer Bonding and Interadsorbate Interactions*, 2021.
(68) Käfer, D.; Witte, G. Evolution of pentacene films on Ag(1 1 1): Growth beyond the first monolayer. *Chem. Phys. Lett.* **2007**, *442*, 376−383.
(69) Günther, C.; Karl, N.; Pflaum, J.; Strohmaier, R.; Gompf, B.; Eisenmenger, W.; Müller, M.; Müllen, K. LEED, STM, and TDS Studies of Ordered Thin Films of the Rhombus-Shaped Poly-condensed Aromatic Hydrocarbon C54H22, on MoS2, GeS, and Graphite. *Langmuir* **2005**, *21*, 656−665.
(70) Laidler, K. J.; Glasstone, S.; Eyring, H. Application of the Theory of Absolute Reaction Rates to Heterogeneous Processes I. The Adsorption and Desorption of Gases. *J. Chem. Phys.* **1940**, *8*, 659−667.
(71) Peters, B. *Reaction Rate Theory and Rare Events Simulations*; Peters, B., Ed.; Elsevier: Amsterdam, 2017; pp 227−271.
(72) Pedio, M.; Doyle, B.; Mahne, N.; Giglia, A.; Borgatti, F.; Nannarone, S.; Henze, S. K. M.; Temirov, R.; Tautz, F. S.; Casalis, L.; et al. Growth of pentacene on Ag(111) surface: A NEXAFS study. *Appl. Surf. Sci.* **2007**, *254*, 103−107.
(73) Duhm, S.; Bürker, C.; Niederhausen, J.; Salzmann, I.; Hosokai, T.; Duvernay, J.; Kera, S.; Schreiber, F.; Koch, N.; Ueno, N.; et al. Pentacene on Ag(111): Correlation of Bonding Distance with Intermolecular Interaction and Order. *ACS Appl. Mater. Interfaces* **2013**, *5*, 9377−9381.
(74) Tao, Y.; Mao, H.; Zhang, H.; He, P. Electronic properties and adsorption structures of tetracene on the Ag(110) surface. *Surf. Sci.* **2015**, *641*, 135−140.
(75) Kafer, D. Characterization and Optimization of Growth and Electronic Structure of Organic Thin Films for Applications in Organic Electronics. Ph.D. thesis; Ruhr-University Bochum, 2008.
(76) Baldacchini, C.; Mariani, C.; Betti, M. G. Adsorption of pentacene on filled d-band metal surfaces: Long-range ordering and adsorption energy. *J. Chem. Phys.* **2006**, *124*, 154702.
(77) Götzen, J.; Käfer, D.; Wöll, C.; Witte, G. Growth and structure of pentacene films on graphite: Weak adhesion as a key for epitaxial film growth. *Phys. Rev. B: Condens. Matter Mater. Phys.* **2010**, *81*, 085440.

https://doi.org/10.1021/acs.jpcc.1c01350
J. Phys. Chem. C 2021, 125, 11166−11174